

## **General Disclaimer**

### **One or more of the Following Statements may affect this Document**

- This document has been reproduced from the best copy furnished by the organizational source. It is being released in the interest of making available as much information as possible.
- This document may contain data, which exceeds the sheet parameters. It was furnished in this condition by the organizational source and is the best copy available.
- This document may contain tone-on-tone or color graphs, charts and/or pictures, which have been reproduced in black and white.
- This document is paginated as submitted by the original source.
- Portions of this document are not fully legible due to the historical nature of some of the material. However, it is the best reproduction available from the original submission.

# NASA Technical Memorandum

(NASA-TM-86511) HUBBLE SPACE TELESCOPE:  
NASA TM-8 POINTING ERROR EFFECTS ON NONLINEAR BALL  
JOINTS (NASA) 25 p HC A02/MF A01 CSCI 03A

N85-32058

Unclas  
G3/89 21797

## HUBBLE SPACE TELESCOPE - POINTING ERROR EFFECTS OF NONLINEAR BALL JOINTS

By John E. Farmer and Floyd R. Grissett

Systems Dynamics Laboratory  
Science and Engineering Directorate

June 1985



National Aeronautics and  
Space Administration

George C. Marshall Space Flight Center

1. REPORT NO. NASA TM-86511		2. GOVERNMENT ACCESSION NO.		3. RECIPIENT'S CATALOG NO.	
4. TITLE AND SUBTITLE Hubble Space Telescope - Pointing Error Effects on Nonlinear Ball Joints				5. REPORT DATE June 1985	
				6. PERFORMING ORGANIZATION CODE	
7. AUTHOR(S) John E. Farmer and Floyd R. Grissett				8. PERFORMING ORGANIZATION REPORT #	
9. PERFORMING ORGANIZATION NAME AND ADDRESS George C. Marshall Space Flight Center Marshall Space Flight Center, Alabama 35812				10. WORK UNIT NO.	
				11. CONTRACT OR GRANT NO.	
12. SPONSORING AGENCY NAME AND ADDRESS National Aeronautics and Space Administration Washington, D.C. 20546				13. TYPE OF REPORT & PERIOD COVERED Technical Memorandum	
				14. SPONSORING AGENCY CODE	
15. SUPPLEMENTARY NOTES Prepared by Systems Dynamics Laboratory, Science and Engineering Directorate.					
16. ABSTRACT  The purpose of this report is to examine the Hubble Space Telescope pointing error produced by optical benches mounted on free ball joints. Spacecraft cable connections are assumed to produce translational and rotational damping and restoring forces which act through the optical bench center of mass. The nonlinear dynamics are modeled and then implemented using an existing computer program for simulating the vehicle dynamics and pointing control system algorithm. Results are presented for the test case which indicate acceptable performance.					
17. KEY WORDS Pointing Control, Optical Bench, Pointing Error, Ball Joint, Cavity, Nonlinear Dynamics, Bench Rotation			18. DISTRIBUTION STATEMENT  Unclassified - Unlimited		
19. SECURITY CLASSIF. (of this report) Unclassified		20. SECURITY CLASSIF. (of this page) Unclassified		21. NO. OF PAGES 24	
				22. PRICE NTIS	

## TABLE OF CONTENTS

	Page
INTRODUCTION AND OBJECTIVES.....	1
EQUATIONS OF MOTION .....	2
CABLE CONNECTIONS .....	9
SIMPLIFYING ASSUMPTIONS.....	14
INPUT DATA AND PROGRAM RESULTS .....	15
CONCLUSIONS .....	16

PRECEDING PAGE BLANK NOT FILMED

## LIST OF ILLUSTRATIONS

Figure	Title	Page
1.	Optical Bench/Spacecraft simplified diagram .....	1
2.	Optical Bench mounting arrangement .....	2
3.	Mass center and cavity center parameters .....	3
4.	Translational and rotational impedance .....	6
5.	System block diagram. ....	8
6.	Translational model .....	9
7.	Rotational model .....	11
8.	Rotation about $V_2$ axis with rigid body dynamics .....	17
9.	Rotation about $V_2$ axis with flexible body dynamics .....	17
10.	$V_2$ axis error with rigid body dynamics. ....	18
11.	$V_2$ axis error with flexible body dynamics .....	18
12.	Rotation about $V_1$ axis with rigid body dynamics .....	19
13.	Rotation about $V_1$ axis with flexible body dynamics .....	19
14.	Rotation about $V_3$ axis with rigid body dynamics .....	20
15.	Rotation about $V_3$ axis with flexible body dynamics .....	20

## TECHNICAL MEMORANDUM

### HUBBLE SPACE TELESCOPE – POINTING ERROR EFFECTS OF NONLINEAR BALL JOINTS

#### INTRODUCTION AND OBJECTIVES

The extreme pointing accuracy of the Hubble Space Telescope (HST) requires the consideration of effects not normally included when performing a Pointing Control System (PCS) analysis. For this reason, an effort has been made to model those mechanisms which could possibly cause very small limit cycles, on the order of 1 milli-arc-sec. The method chosen to mount the Scientific Instrument (SI) Optical Benches on-board the HST provide one such mechanism.

While the primary concern was for the HST, the program used for this analysis was written in modular form and can, therefore, be applied to other spacecraft. As shown in Figure 1, the mathematical model for the Optical Bench receives only the vehicle angular body rates and the spacecraft to inertial frame transformation. These variables are processed and returned to the main program as reactive torques affecting the attitude control system performance. It is assumed for purposes of this study that the spacecraft is operating under drag free conditions. However, an input for external forces (such as atmospheric resistance) has been provided to satisfy the more general situation of a vehicle experiencing and reacting to various external disturbances.

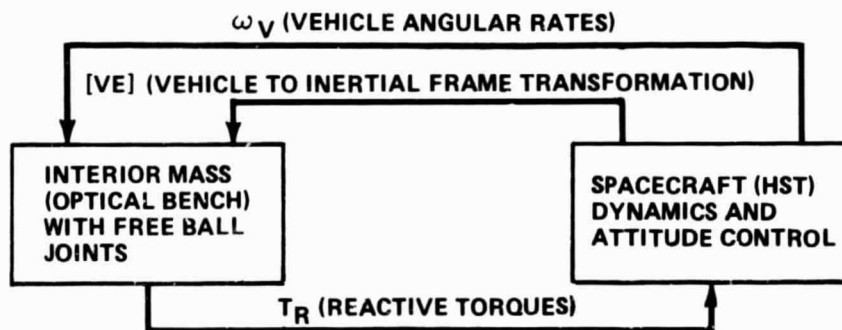


Figure 1. Optical Bench/Spacecraft simplified diagram.

There were three primary objectives to be accomplished by this study:

- 1) Define the nonlinear dynamics associated with the SI Optical Benches mounted on free ball joints.
- 2) Develop a computer program describing these dynamics.
- 3) Combine this program with an existing HST simulation to determine the effects on vehicle pointing accuracy.

## EQUATIONS OF MOTION

The optical benches were assumed to be mounted as shown in Figure 2.

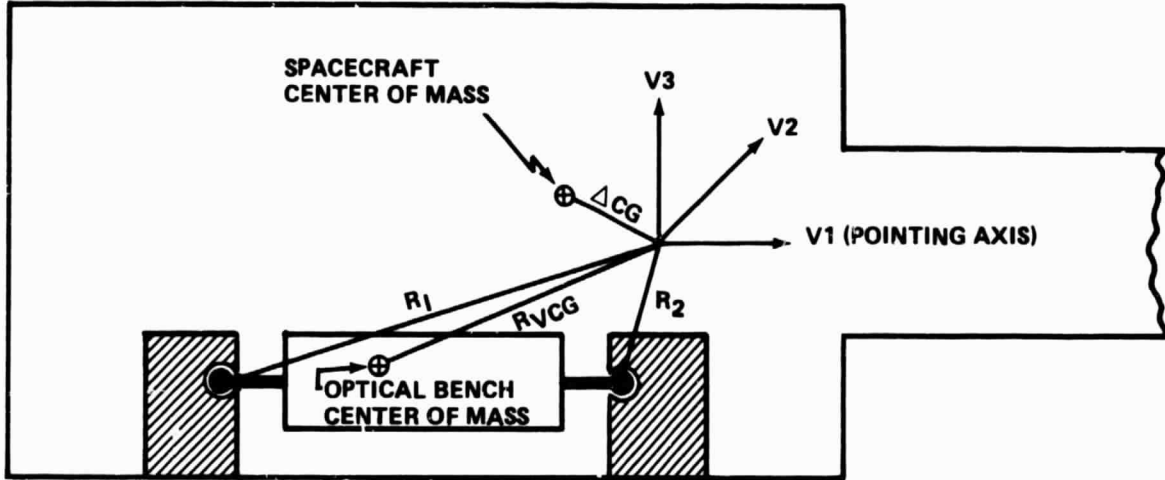


Figure 2. Optical Bench mounting arrangement.

The variables  $\Delta CG$ ,  $R_1$ ,  $R_2$ ,  $R_{VCG}$  are defined in the body-fixed frame ( $V_1$ ,  $V_2$ ,  $V_3$ ) to be

$$\Delta CG = \begin{bmatrix} \Delta CG_{V1} \\ \Delta CG_{V2} \\ \Delta CG_{V3} \end{bmatrix} ; R_{VCG} = \begin{bmatrix} R_{CGV1} \\ R_{CGV2} \\ R_{CGV3} \end{bmatrix} \quad (1)$$

$$R_1 = \begin{bmatrix} R_{1V1} \\ R_{1V2} \\ R_{1V3} \end{bmatrix} ; R_2 = \begin{bmatrix} R_{2V1} \\ R_{2V2} \\ R_{2V3} \end{bmatrix}$$

The vectors  $R_1$  and  $R_2$  represent the distance to the geometric center of the aft and forward cavities (sockets), respectively. The distance from the vehicle center of mass (CM) to each cavity center and the optical bench CM is depicted in Figure 3 and is expressed by equation (2).

$$R_F = R_2 - \Delta CG \text{ (Forward Cavity)} \quad (2)$$

$$R_A = R_1 - \Delta CG \text{ (Aft Cavity)}$$

(2)  
(Conc.)

$$R_{CG} = R_{VCG} - \Delta CG \text{ (Optical Bench CM)}$$

Let the vehicle angular rates be represented by

$$\omega_V = \begin{bmatrix} \omega_{V1} \\ \omega_{V2} \\ \omega_{V3} \end{bmatrix} \quad (\text{RAD/SEC}) \quad (3)$$

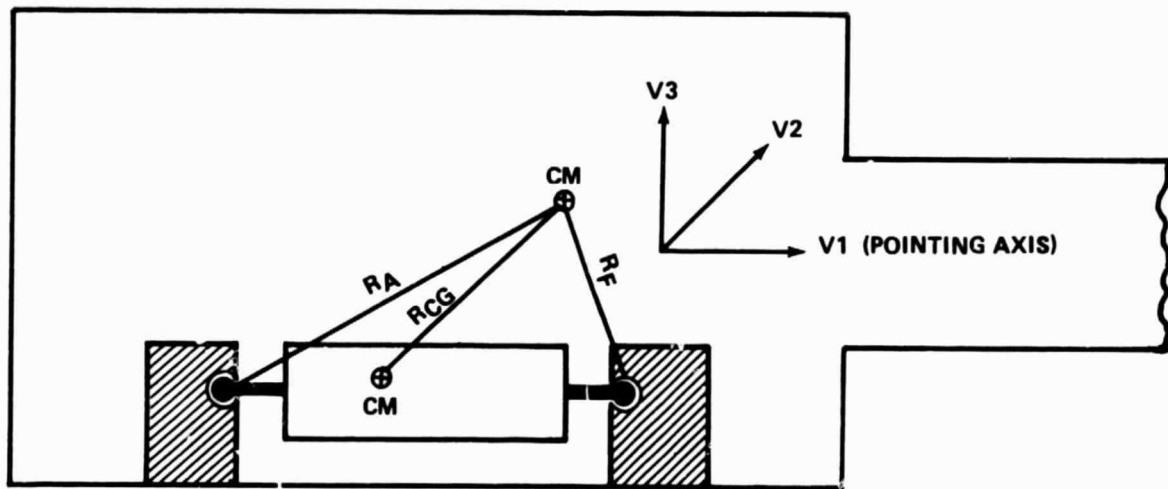


Figure 3. Mass center and cavity center parameters.

In one computational period (specified by  $\Delta t$  sec) these rates cause the center point of each cavity to sweep out an arc of length

$$\Delta S_F = R_F \omega_V \Delta t \quad (4)$$

$$\Delta S_A = R_A \omega_V \Delta t \quad .$$

Expressing equation (4) in matrix notation produces

$$\Delta S_F = [-\tilde{R}_F] [\omega_V] \Delta t \quad (5)$$

$$\Delta S_A = [-\tilde{R}_A] [\omega_V] \Delta t \quad .$$



where the tilde operation for any vector

$$A = \begin{bmatrix} X \\ Y \\ Z \end{bmatrix} \quad (6)$$

is defined to be

$$[A] = \begin{bmatrix} 0 & -Z & Y \\ Z & 0 & -X \\ -Y & X & 0 \end{bmatrix} \quad (7)$$

Applying the definition [equation (7)] to equation (5) gives

$$\Delta S_F = \begin{bmatrix} 0 & R_{FV3} & -R_{FV2} \\ -R_{FV3} & 0 & R_{FV1} \\ R_{FV2} & -R_{FV1} & 0 \end{bmatrix} \begin{bmatrix} \omega_{V1} \\ \omega_{V2} \\ \omega_{V3} \end{bmatrix} \Delta t \quad (8)$$

$$\Delta S_A = \begin{bmatrix} 0 & R_{AV3} & -R_{AV2} \\ -R_{AV3} & 0 & R_{AV1} \\ R_{AV2} & -R_{AV1} & 0 \end{bmatrix} \begin{bmatrix} \omega_{V1} \\ \omega_{V2} \\ \omega_{V3} \end{bmatrix} \Delta t$$

Let [EV] be the vehicle to inertial frame coordinate transformation. Then the arc lengths expressed in inertial space are

$$\begin{aligned} \Delta S_F &= [EV] [-\tilde{R}_F] [\omega_V] \Delta t \\ \Delta S_A &= [EV] [-\tilde{R}_A] [\omega_V] \Delta t \end{aligned} \quad (9)$$

The sum of the external and internal forces acting on the spacecraft are represented by

$$F = \begin{bmatrix} F_{V1} \\ F_{V1} \\ F_{V3} \end{bmatrix} \quad (10)$$

The body fixed forces given by equation (10) produce vehicle accelerations in the inertial coordinate frame given by

$$A_I = [EV] \frac{F}{M_V} \quad (11)$$

where  $M_V$  is the weight of the vehicle expressed in kilograms. Therefore, the average inertial translational velocity of each cavity center during a single computational period is

$$V_{AVG} = V + \frac{A_I}{2} \Delta t \quad (12)$$

and the inertial distance traversed in one time period is given by

$$\Delta D = V_{AVG} \Delta t \quad (13)$$

The total displacement of each cavity center can now be expressed as

$$C_F = \sum_{i=1}^{t_f/\Delta t} (\Delta S_F + \Delta D)_i \quad (14)$$

$$C_A = \sum_{i=1}^{t_f/\Delta t} (\Delta S_A + \Delta D)_i$$

where  $t_f$  is the total time period being considered.

Now consider the inertial ball displacements  $B_F$  and  $B_A$ . Let the inertial frame three-axis angular rates of the Optical Bench be defined by  $[\dot{\beta}_I]$ . Referring to Figure 4 the arc lengths traversed by each ball in one time period are defined by

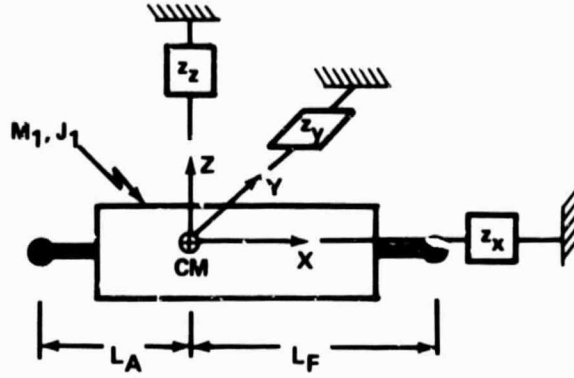


Figure 4. Translational and rotational impedance.

$$\Delta K_F = [-\tilde{L}_F] [\dot{\beta}_I] \Delta t$$

$$\Delta K_A = [-\tilde{L}_A] [\dot{\beta}_I] \Delta t$$
(15)

Also, let the inertial translation of the Optical Bench center-of-mass in one time period be defined by the symbol  $\Delta D_T$ . The total displacement of each ball can now be described as

$$B_F = \sum_{i=1}^{t_f/\Delta t} (\Delta K_F + \Delta D_T)_i$$

$$B_A = \sum_{i=1}^{t_f/\Delta t} (\Delta K_A + \Delta D_T)_i$$
(16)

The magnitude of the force acting on each ball due to cavity wall contact is specified by

$$|F_F| = K_1 [|C_F - B_F| - \text{TOL}_F]$$

$$|F_A| = K_2 [|C_A - B_A| - \text{TOL}_A]$$
(17)

where

$K_1$  = spring constant for forward ball. This constant represents the restoring force which acts when the forward ball contacts the cavity wall.

$K_2$  = spring constant for aft ball.

$TOL_F$  = forward ball dead zone. This constant represents the free space (or tolerance) between the forward ball and the cavity wall.

$TOL_A$  = aft ball dead zone.

The quantity within the brackets of equation (17) represents the magnitude of the compression (extension is not possible) of the respective springs, i.e., this is the distance the ball "sinks" into the cavity wall before the generated force can restore the ball to the free space. Equation (17) acts only after cavity wall contact has been made and becomes zero after contact has been lost according to equation (18)

$$\begin{aligned} |F_F| &= 0 & |C_F - B_F| &\leq TOL_F \\ &\text{for} & & \\ |F_A| &= 0 & |C_A - B_A| &\leq TOL_A \end{aligned} \quad (18)$$

A simplifying assumption has been made that no tangential forces can be exerted on the balls due to wall contact. Therefore, the forces are always directed from each ball toward the center of the cavity. The unit vectors expressing the direction of the forces  $F_F$  and  $F_A$  are given by

$$\begin{aligned} U_F &= \frac{(C_F - B_F)}{|C_F - B_F|} \\ U_A &= \frac{(C_A - B_A)}{|C_A - B_A|} \end{aligned} \quad (19)$$

Each ball force (expressed in the inertial frame) can now be represented as

$$\begin{aligned} F_F &= |F_F|U_F \\ F_A &= |F_A|U_A \end{aligned} \quad (20)$$

The system block diagram shown in Figure 5 gives a more complete definition of this logic.



**Figure 5. System block diagram.**

## CABLE CONNECTIONS

Each Optical Bench is connected to the spacecraft through electrical cables used for power and scientific data transmission. These cables will have an effect on the motion of the Optical Bench since they have properties which produce translational and rotational spring and damping coefficients. The cable forces and torques are assumed to act through the Optical Bench center of mass as depicted in Figure 4. Let the mass and inertia tensor be defined by  $M_1$  and

$$J_1 = \begin{bmatrix} J_{V1} & 0 & 0 \\ 0 & J_{V2} & 0 \\ 0 & 0 & J_{V3} \end{bmatrix} \quad (21)$$

Establish the  $x, y, z$  coordinate frame with origin at the Optical Bench center of mass and with axes initially parallel to the vehicle and inertial frames. The lever arms  $L_A$  and  $L_F$  are (referring to Figs. 1 and 4)

$$L_A = R_1 - R_{VCG} \quad (22)$$

$$L_F = R_2 - R_{VCG}$$

The cable dynamics are shown in Figure 4 as an impedance ( $z_x, z_y, z_z$ ) in each axis connecting the Optical Bench center of mass and the spacecraft.

Consider first the translational dynamics. A mechanical representation used for equation derivation is shown in Figure 6 and has been simplified (for ease of drawing) such that the attach point lever

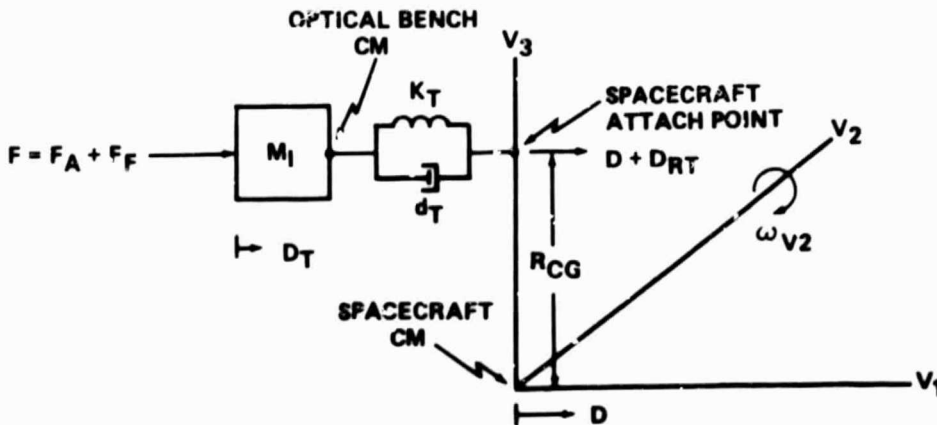


Figure 6. Translational model.

arm lies only along the  $V_3$  axis. Consider the vehicle to have an angular rate ( $\omega_{V2}$ ) about the  $V_2$  axis and a translation ( $D$ ) along the  $V_1$  axis. Under these conditions, the motion of the attach point is given by the sum of  $D$  and  $D_{RT}$  where

$$D_{RT} = \int V_{RT} dt = - \int R_{CG} \omega_{V2} dt \quad (23)$$

Expressing this in the more general three-dimensional case and in matrix notation gives

$$\dot{D}_{RT} = V_{RT} = [-\tilde{R}_{CG}] \omega_V \quad (24)$$

Writing the transfer function from the input force  $F$  to the attach point produces,

$$F = M_1 \ddot{D}_T + d_T (\dot{D}_T - \dot{D}_{RT} - \dot{D}) + K_T (D_T - D_{RT} - D) \quad (25)$$

Rearranging equation (25) and introducing LaPlace notation gives

$$F = (M_1 S^2 + d_T S + K_T) D_T - (d_T S + K_T) D_{RT} - (d_T S + K_T) D \quad (26)$$

If it is assumed that the variables  $D_{RT}$  and  $D$  are zero (as would be the case for a stationary vehicle) then equation (26) simplifies to

$$\frac{D_T}{F} = \frac{1/M_1}{S^2 + d_T/M_1 S + K_T/M_1} = \frac{1/M_1}{S^2 + 2\xi \omega_N S + \omega_N^2} \quad (27)$$

For the purpose of this report it was assumed that the spring constant ( $K_T$ ) and damping ratio ( $\xi$ ) were

$$K_T = 1 \text{ lb/in.} = 175.118 \text{ N/m} \quad \text{and} \quad \xi = 0.005 \text{ (unitless).}$$

With these assumptions the natural frequency and damping coefficient are calculated to be

$$f = 0.174 \text{ Hz} \quad \text{and} \quad d_T = 1.6 \text{ N-S/m}$$

Since the Optical Bench mass is invariant all of the translational coefficients will be the same for all vehicle axes.

A simplified view of the mechanical model used for rotational equation derivation is shown in Figure 7.

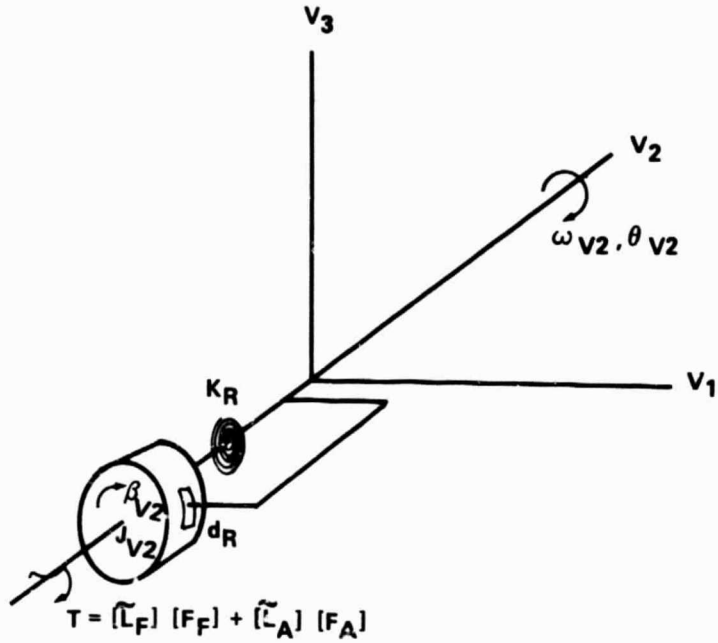


Figure 7. Rotational model.

The torque applied to the Optical Bench inertia [equation (21)] due to wall contact is

$$T = [\tilde{L}_F] [F_F] + [\tilde{L}_A] [F_A] \quad , \quad (28)$$

where  $L_A$  and  $L_F$  are defined in Figure 4.

Summation of the torques on each inertia produces the following equation,

$$T = J_1 \ddot{\beta}_Z + d_R (\dot{\beta}_Z - \omega_V) + K_R (\beta - \theta) \quad , \quad (29)$$

where

$$\beta_I = \begin{bmatrix} \beta_{V1} \\ \beta_{V2} \\ \beta_{V3} \end{bmatrix} ; \quad \theta = \begin{bmatrix} \theta_{V1} \\ \theta_{V2} \\ \theta_{V3} \end{bmatrix} \quad , \quad (30)$$

are the rotation angles of the Optical Bench and the vehicle, respectively.

Again introducing LaPlace notation and letting  $\omega_V = \theta = 0$  produces



$$\frac{\beta}{T} = \frac{J_1^{-1}}{s^2 + d_R/J_1 s + K_R/J_1} = \frac{J_1^{-1}}{s^2 + 2\zeta\omega_N s + \omega_N^2} \quad (31)$$

With the assumption that

$$K_R = 1.3558 \frac{\text{N}\cdot\text{m}}{\text{RAD}}$$

$$\zeta = 0.005 \text{ unitless}$$

the following constants are calculated

$$d_R = \begin{bmatrix} 0.0877 \\ 0.1431 \\ 0.1431 \end{bmatrix} (\text{N}\cdot\text{m}\cdot\text{S}) \quad ; \quad f_N = \begin{bmatrix} 0.0246 \\ 0.0151 \\ 0.0151 \end{bmatrix} (\text{Hz})$$

The forces  $F_A$  and  $F_F$  are calculated in the inertial frame; however, the translational and rotational spring and damping constants only have meaning in the vehicle reference axis system. Consequently, the forces and torques generated as a result of motional differences between the vehicle and Optical Bench must be converted into the vehicle frame and back to the inertial frame. Equation (25) can be written as

$$\ddot{D}_T = \frac{1}{M_1} [F + F_{\text{DAMP}} + F_S] \quad , \quad (32)$$

where

$$F_{\text{DAMP}} = d_T(\dot{D} + \dot{D}_{RT} - \dot{D}_T) = d_T(V - V_T + V_{RT}) \quad (33)$$

$$F_S = K_T(D - D_T + D_{RT})$$

Since the spring and damping factors can be applied only in the vehicle frame, equation (33) must be rewritten as

$$F_{DAMP} = [EV] \left\{ [d_T] \times ([VE] [V - V_T] + V_{RT}) \right\}$$

$$F_S = [EV] \left\{ [K_T] \times ([VE] [D - D_T] + D_{RT}) \right\}$$

where  $[VE] = [EV]^T$  = vehicle to inertial frame transformation.

For the rotational dynamics, equation (29) is expressed as

$$\ddot{\beta} = J_I^{-1} [T + T_{DAMP} + T_S]$$

where

$$T_{DAMP} = d_R [\omega_V - \dot{\beta}]$$

$$T_S = K_R [\theta - \beta]$$

(36)

Again converting to the vehicle frame and back to the inertial reference gives

$$T_{DAMP} = [EV] \left\{ d_R \times (\omega_V - [VE] [\dot{\beta}_I]) \right\}$$

$$T_S = [EV] \left\{ K_R \times (\theta_V - [VE] [\beta_I]) \right\}$$

(37)

Equations (34) and (37) represent the dynamics as implemented and as shown in the block diagram (Fig. 5).

Referring to equation (11) the vehicle acceleration can now be expressed in more detail by

$$A_I = \frac{[EV] [F]}{M_V} = - \frac{[F_A + F_F + F_{DAMP} + F_S - (\text{EXTERNAL FORCES})]}{M_V}$$

(38)

It is possible for the Optical Bench to transmit reactive torques to the vehicle through three different paths:

- 1) Forward and aft wall contact forces acting through their respective lever arms.
- 2) Optical Bench rotational damping and spring torques.
- 3) Translational spring and damping forces acting at the Optical Bench attach point.

The total reactive torque (in vehicle coordinates) can now be expressed as

$$\mathbf{T}_R = -[\mathbf{VE}] \left\{ [\tilde{\mathbf{R}}_F] [\mathbf{F}_F] + [\tilde{\mathbf{R}}_A] [\mathbf{F}_A] + [\tilde{\mathbf{R}}_{CG}] [\mathbf{F}_{DAMP} + \mathbf{F}_S] + \mathbf{T}_{DAMP} + \mathbf{T}_S \right\}. \quad (39)$$

Equation (39) represents the reactive torques that drive the spacecraft attitude control system.

### SIMPLIFYING ASSUMPTIONS

All the necessary equations have been derived and the loop can now be closed through equation (39) as shown in Figure 5. Certain simplifying assumptions have been made in the equation derivation either because their effects were considered to be negligible or because the data for their implementation was not available.

- 1) The arc lengths  $\Delta S$ ,  $\Delta D_T$ , and  $\Delta K$  were considered to be straight lines instead of curved paths.
- 2) No tangential forces are exerted on the Optical Bench balls by cavity wall contact. Contact forces are always directed along a line through the contact point and the cavity center.
- 3) Cable damping and spring constants for rotation and translation act through the Optical Bench center of mass.
- 4) The Optical Bench inertia tensor was considered to be diagonal (i.e., all coupling terms were zero).
- 5) The ball and socket dead zones (specified by  $TOL_F$  and  $TOL_A$ ) are small enough to allow the Optical Bench reference frame to be considered congruent with the vehicle frame.
- 6) The total torque on the Optical Bench is expressed by

$$\mathbf{T}_T = \mathbf{J}_1 \ddot{\boldsymbol{\beta}} + (\dot{\boldsymbol{\beta}} \times \mathbf{H})$$

where  $\mathbf{H}$  is the angular momentum. Assuming a diagonal inertia tensor and small angular rates, the term  $(\dot{\boldsymbol{\beta}} \times \mathbf{H})$  can be ignored.

- 7) The ball contact spring stiffness was assumed to be constant.
- 8) The Optical Bench was assumed to be rigid.

## INPUT DATA AND PROGRAM RESULTS

The Faint Object Camera (FOC) is the only Scientific Instrument on board the HST which has the ball and socket mounting arrangement at each end. Referring to Figure 2 the variables shown for the FOC are given by (all units are in meters)

$$\Delta CG = \begin{bmatrix} 6.617 \\ 0.005 \\ -0.145 \end{bmatrix} ; \quad R_{VCG} = \begin{bmatrix} 4.461 \\ -0.297 \\ -0.325 \end{bmatrix} ; \quad R_1 = \begin{bmatrix} 3.1 \\ -0.102 \\ -0.102 \end{bmatrix} ; \quad R_2 = \begin{bmatrix} 5.125 \\ -0.7 \\ -0.7 \end{bmatrix}$$

Combining the data in Figure 2 according to previously developed equations produces the variables of Figure 3

$$R_A = \begin{bmatrix} -3.517 \\ -0.107 \\ 0.043 \end{bmatrix} ; \quad R_{CG} = \begin{bmatrix} -2.156 \\ -0.302 \\ -0.18 \end{bmatrix} ; \quad R_F = \begin{bmatrix} -1.492 \\ -0.705 \\ -0.555 \end{bmatrix}$$

and Figure 4

$$L_A = \begin{bmatrix} -1.361 \\ 0.195 \\ 0.233 \end{bmatrix} ; \quad L_F = \begin{bmatrix} 0.664 \\ -0.403 \\ -0.375 \end{bmatrix}$$

The FOC mass and inertia terms are defined by

$$M_1 = 146 \text{ Kg}$$

and

$$J_1 = \begin{bmatrix} 7.256 & 0 & 0 \\ 0 & 39.207 & 0 \\ 0 & 0 & 39.207 \end{bmatrix} \text{ Kg m}^2$$

where  $J_1$  is given about the FOC center of mass.

As a test case the vehicle was maneuvered 0.05 deg about the positive  $V_2$  axis. This rotation was sufficient to cause an aft cavity wall collision. The system performance was examined with and without flexible body dynamics. The rotation about the  $V_2$  (maneuver axis) produced very similar results in each case as shown in Figures 8 and 9. Each plot shows a rotation to 0.05 deg (180 arc-sec) but the scale is such that the small variations due to body bending are not evident. Plotting the angular error in the maneuver axis produces Figures 10 and 11. The maneuver takes approximately 80 sec to complete. The small variations in each plot are less than 1 milli-arc-sec and are principally due to the translational and rotational dynamics of the suspended mass. Flexible body effects are much more pronounced in Figures 12 through 15 which represent the angular rotations for the  $V_1$  and  $V_3$  axes. Collisions between the aft ball and the cavity wall are most evident in Figures 14 and 15 which indicate six collisions of the aft ball at 14, 22, 26, 54, 62, and 67 sec. After the maneuver has been completed, the flexible body effects are once again very small and the variations can be attributed primarily to mass translation.

### CONCLUSIONS

The simulation results indicate that there is no strong coupling from the wall/ball collisions into the vehicle elastic body. Flexible body "ringing" soon damps out after the vehicle rotation has been accomplished and the last collision has occurred. Pointing axis deviations as determined from the RMS value of the  $V_2$  and  $V_3$  axis rotations are less than  $1 \times 10^{-3}$  arc-sec. The principal cause of the damped vibration seen beginning at 80 sec is the translational effects of the Optical Bench acting through the cable connections. Studies will continue to determine if uncertainties in flexible body and translational mode frequencies could cause an instability or limit cycle condition to exist.

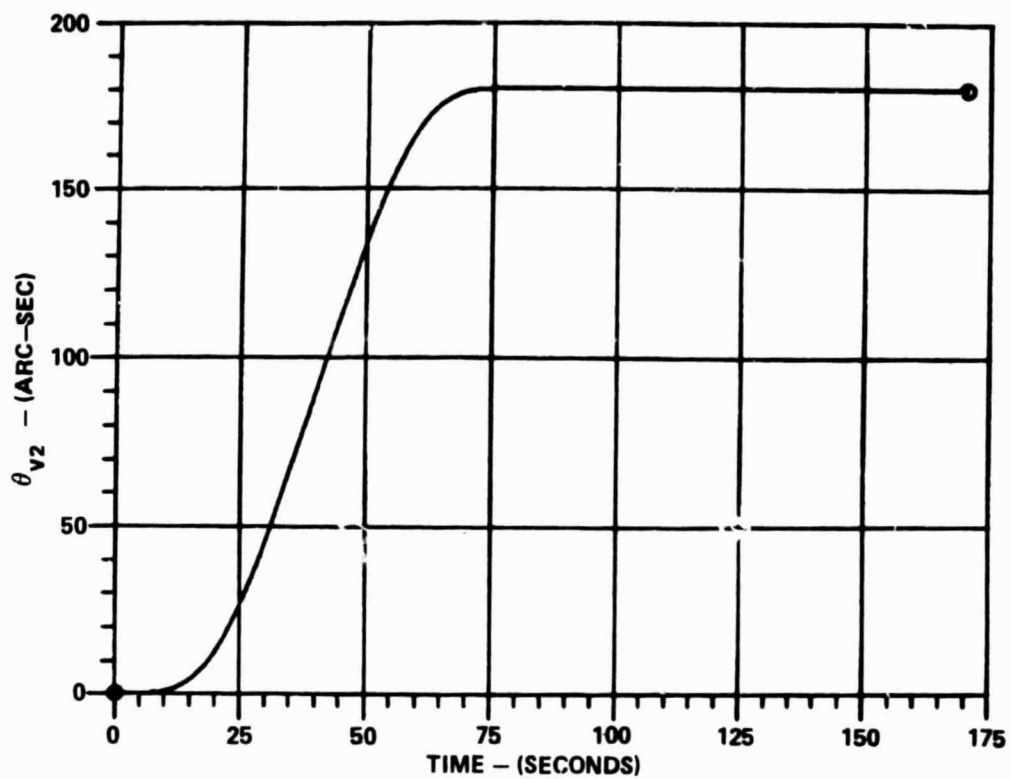


Figure 8. Rotation about  $V_2$  axis with rigid body dynamics.

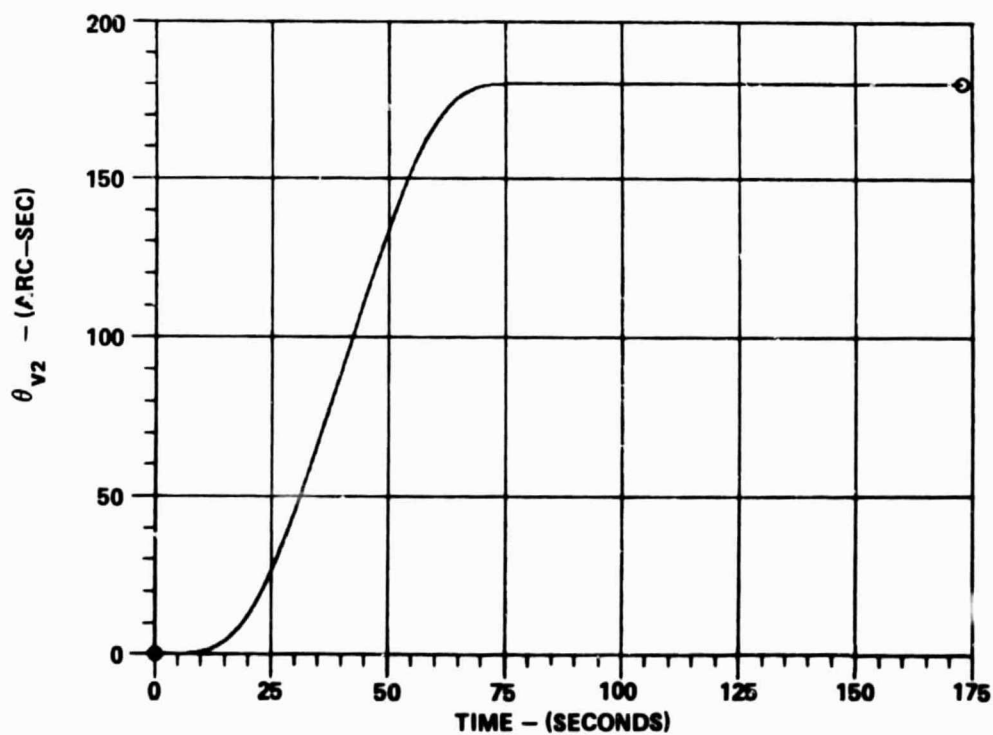


Figure 9. Rotation about  $V_2$  axis with flexible body dynamics.

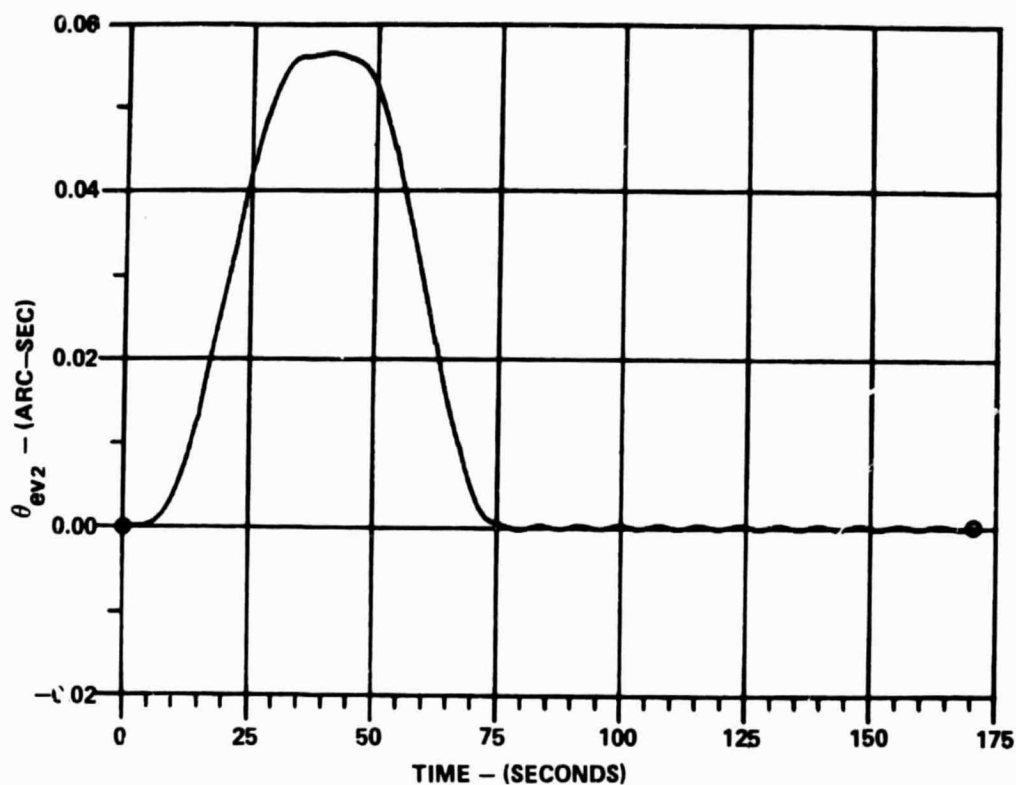


Figure 10. V<sub>2</sub> axis error with rigid body dynamics (difference between commanded and actual vehicle angle).

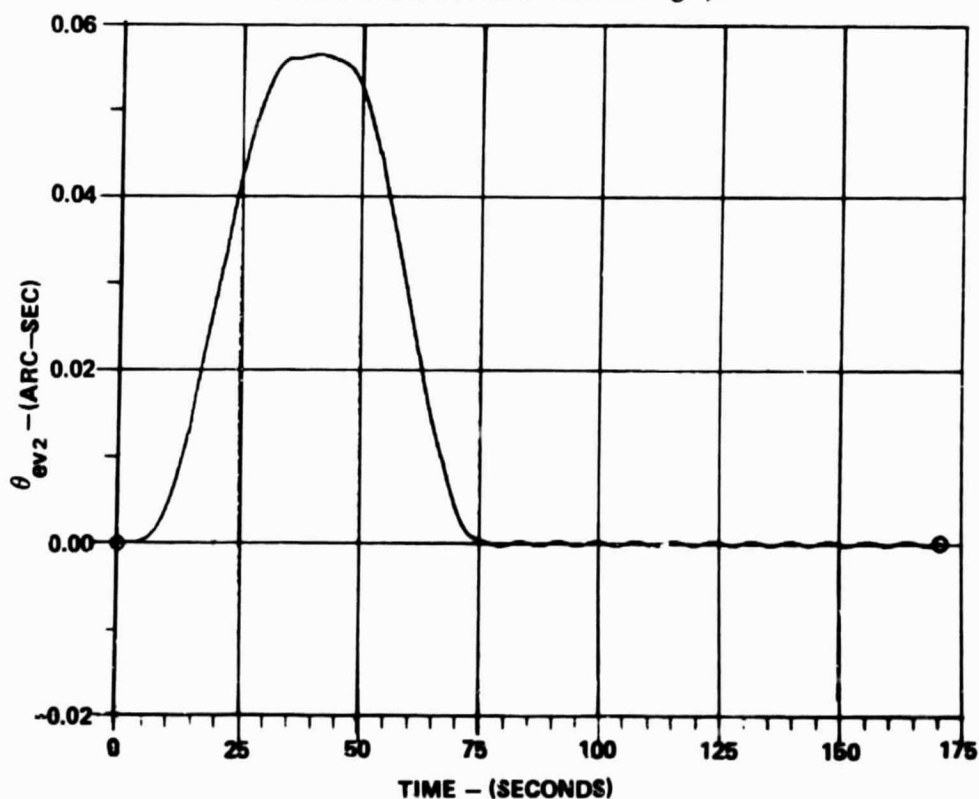


Figure 11. V<sub>2</sub> axis error with flexible body dynamics (difference between commanded and actual vehicle angle).

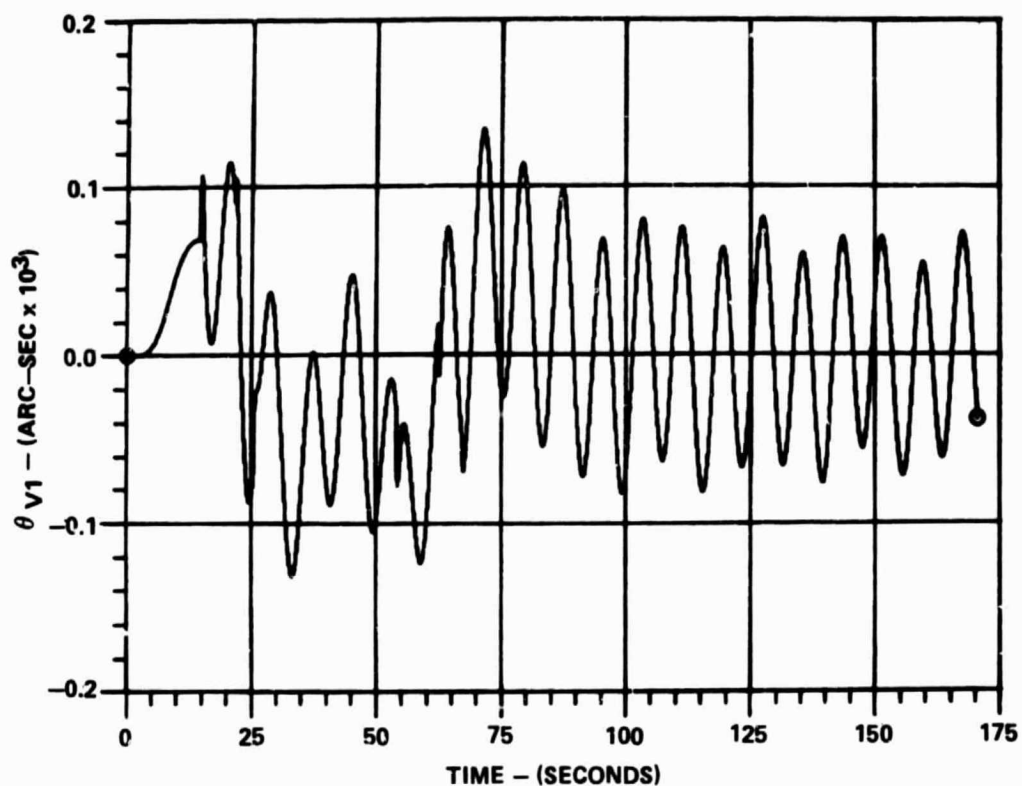


Figure 12. Rotation about  $V_1$  axis with rigid body dynamics.

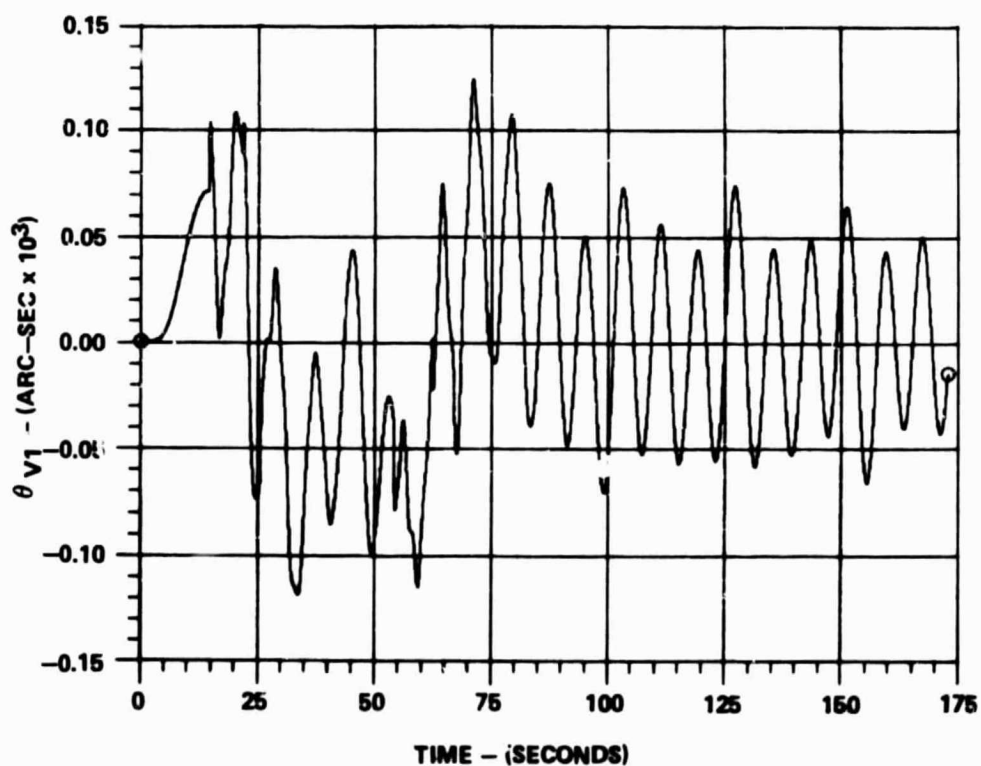


Figure 13. Rotation about  $V_1$  axis with flexible body dynamics.



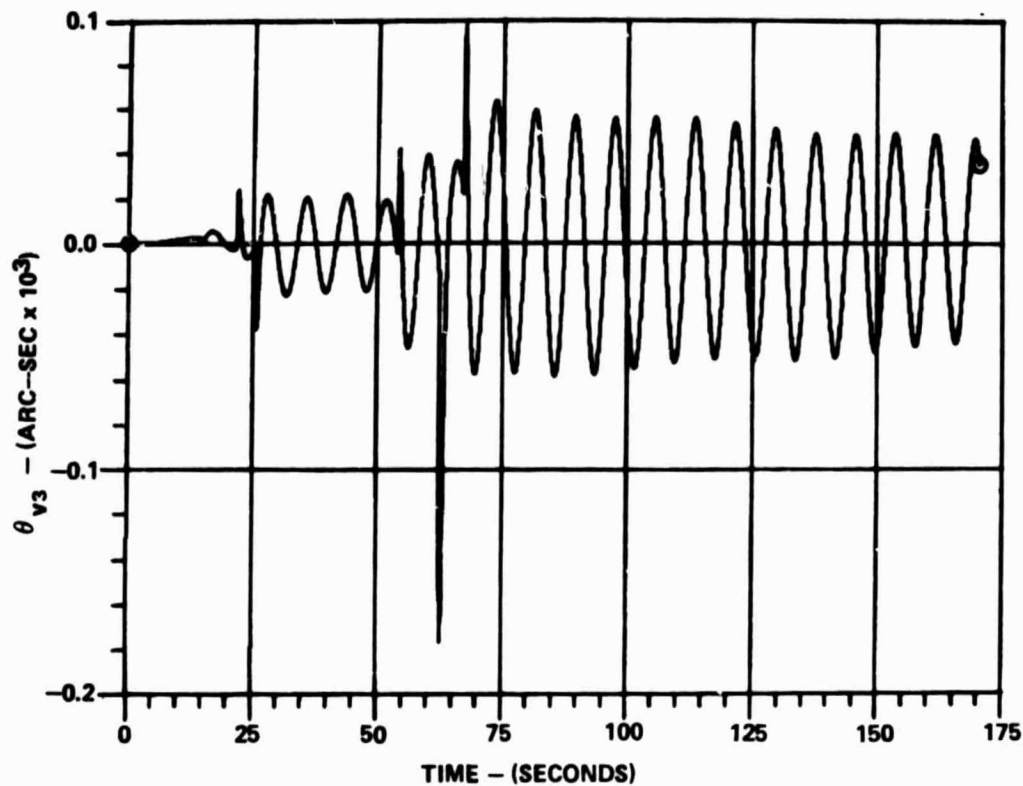


Figure 14. Rotation about  $V_3$  axis with rigid body dynamics.

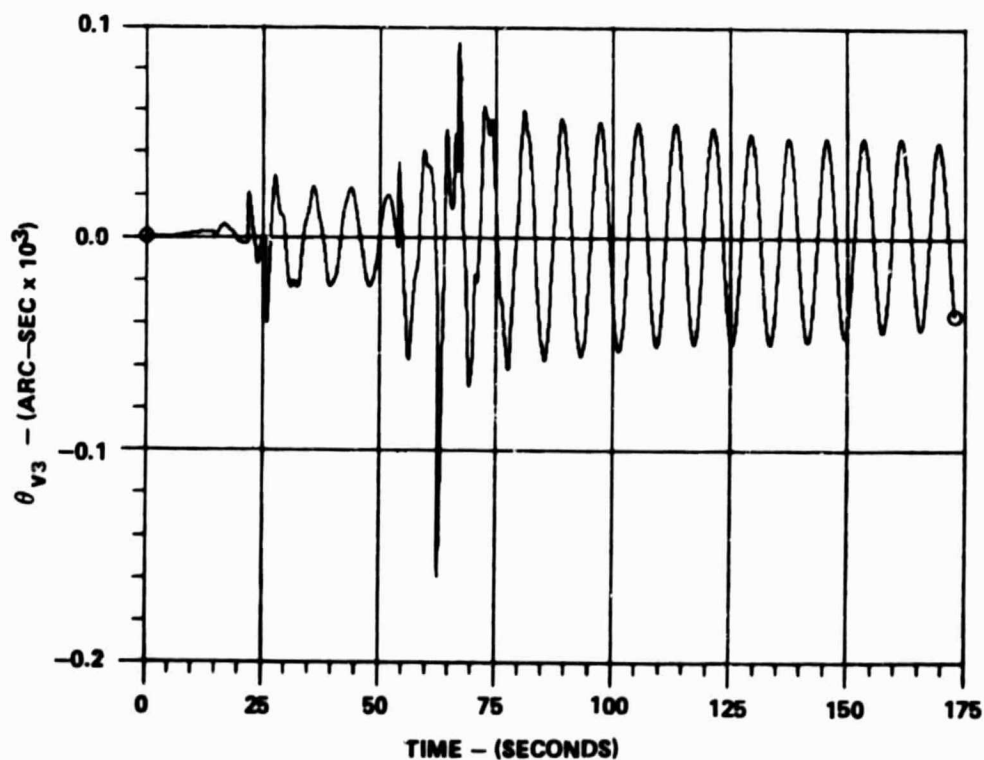


Figure 15. Rotation about  $V_3$  axis with flexible body dynamics.

**APPROVAL**

**HUBBLE SPACE TELESCOPE — POINTING ERROR EFFECTS OF  
NONLINEAR BALL JOINTS**

By John E. Farmer and Floyd R. Grissett

The information in this report has been reviewed for technical content. Review of any information concerning Department of Defense or nuclear energy activities or programs has been made by the MSFC Security Classification Officer. This report, in its entirety, has been determined to be unclassified.



G. F. McDONOUGH  
Director, Systems Dynamics Laboratory